

RESEARCH



Femtosecond tunable-wavelength photoassisted cold field emission

Rudolf Haindl^{1,2} · Kerim Köster^{1,2} · John H. Gaida^{1,2} · Maximilian Franz^{1,2} · Armin Feist^{1,2} · Claus Ropers^{1,2}

Received: 6 July 2022 / Accepted: 6 January 2023

© The Author(s) 2023

Abstract

We demonstrate photoassisted cold field emission (PFE) from a tungsten tip induced by tunable-wavelength low-power femtosecond laser excitation. The emission current from the apex of the (310)-oriented single-crystalline emitter is shown to linearly depend on the incident laser power, while the effective work function is reduced by the respective photon energy. Our results promote the implementation of the linear regime in laser-triggered cold field emission for ultrafast transmission electron microscopy.

1 Introduction

Ultrafast electron microscopy combines high spatial and temporal resolution for the study of non-equilibrium phenomena. In particular, ultrafast transmission electron microscopy (UTEM) offers unique access to structural, electronic and magnetic degrees-of-freedom in nanomaterials, probing ultrafast spin dynamics [1–3], the evolution of strain waves [4–6], structural phase transitions [7–9] and electromagnetic fields [10–15]. The achievable image contrast and resolution are governed by the spatial and temporal electron pulse properties, ultimately determined by the electron source [16–18].

Time-resolved electron microscopy is pursued in various modes, initially implemented using planar photocathodes. Single-shot imaging of irreversible processes is possible in dynamic TEM using high-charge nanosecond electron pulses [19–21]. Stroboscopic imaging of reversible processes facilitates ultrashort temporal resolution in the limit of low bunch charges [16]. Sharp metallic [22–26] and dielectric [27, 28] tips offer a higher spatial coherence of photoelectrons, which has stimulated the development of

laser-triggered field emitters for ultrafast scanning [29] and transmission electron microscopy [18], either using nonlinear photoemission from a cold emitter [11, 30], or linear photoemission [18, 31, 32] based on laser-assisted Schottky field emission [29, 33].

In conventional electron microscopy, the development of high-brightness continuous electron sources has culminated in cold field emitters [34–37]. For applications in UTEM, photoassisted field emission (PFE) from such emitters promises narrow energy spread and freely-tunable electron pulses with superior phase-space density [38]. Nonlinear and linear photocurrents supported by tunneling and the Schottky effect at high static fields were investigated in numerous studies (see, e.g., Refs. [22–26, 29, 30, 39–43]). For femtosecond excitation, electron spectroscopy identified individual single- and multi-photon tunneling emission channels [25]. Using continuous-wave lasers, a photon-energy dependence of the single-photon channel was observed for vacuum tunneling [39, 44] and across the junction of a scanning tunneling microscope [45]. This suggests a wavelength-tunability of the generation of femtosecond electron pulses using PFE in the linear regime.

In this work, we experimentally investigate femtosecond-laser triggered one-photon-assisted photoelectron emission from the apex of W(310) cold field emitters. We study the wavelength- and voltage-dependent photoemission current and the transition between laser-induced and static tunneling, finding excellent agreement of the data with a model invoking Fowler–Nordheim tunneling and a work function reduced by the photon energy.

✉ Armin Feist
armin.feist@mpinat.mpg.de

Claus Ropers
claus.ropers@mpinat.mpg.de

¹ Max Planck Institute for Multidisciplinary Sciences,
37077 Göttingen, Germany

² 4th Physical Institute – Solids and Nanostructures,
Georg-August-Universität Göttingen, 37077 Göttingen,
Germany

2 Photoemission model

Extracting electrons from a solid requires passing the potential barrier into vacuum, either by tunneling or over-the-barrier emission. A variety of processes can trigger photoemission from nanotips including multiphoton [23–25, 46] or above-threshold [47, 48] photoemission, and optical field-driven emission [22, 49–54]. Whereas these optically nonlinear processes offer localization to the apex via field enhancement, the resulting kinetic energy distributions are substantially broadened [47, 51, 55], in addition to stochastic and space-charge Coulomb effects arising at higher currents [56–64].

Linear PFE [39, 44] involves direct photoexcitation and subsequent tunneling through the potential barrier. This mechanism is used in laser-triggered Schottky field emitters [18, 29, 33] that typically operate at elevated temperatures (>1500 K) with sub- μm -source-localization by a facet-specific chemical reduction of the work function. In principle, PFE from cold, i.e., room temperature, field emitters [39] reduces the thermal spread of the Fermi-Dirac distribution and can increase the emitter brightness due to a small virtual source size [26].

For illustration, Fig. 1 compares standard field emission (FE) (panel a) and one-photon-PFE (panel b). Both processes involve direct tunneling through the potential barrier, but for PFE, the emission occurs through a state at higher energy, lowering the effective work function ϕ_λ (see Fig. 1b). This manifests in a linear relation of $\phi_\lambda = \phi - E_\lambda$ with the photon energy $E_\lambda = \frac{hc}{\lambda}$ (h : Planck's constant, c : velocity of light, λ : wavelength of the photoexcitation laser).

Fowler–Nordheim tunneling theory describes the tunneling current through a potential barrier into vacuum [65]. The width and height of the tunneling barrier is reduced by increasing the electric field at the photocathode. For a nanometric tip emitter, the electric field applied by the extraction

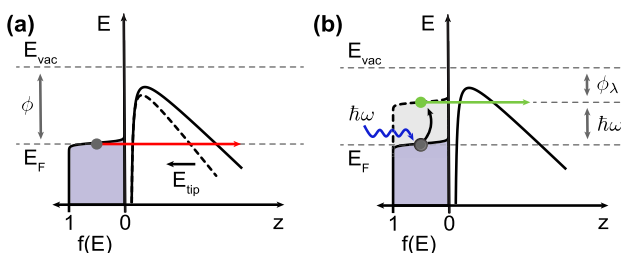


Fig. 1 Electron emission process. Schematic electron energy distribution in the metal (left, Fermi energy level E_F) and potential barrier (right, vacuum energy level E_{vac}). **a** Field emission: Electrons tunnel through the potential barrier, lowered and narrowed by an electric field applied to the tip (dashed line). **b** Photoassisted field emission: Electrons elevated by the photon energy tunnel through an effectively reduced barrier

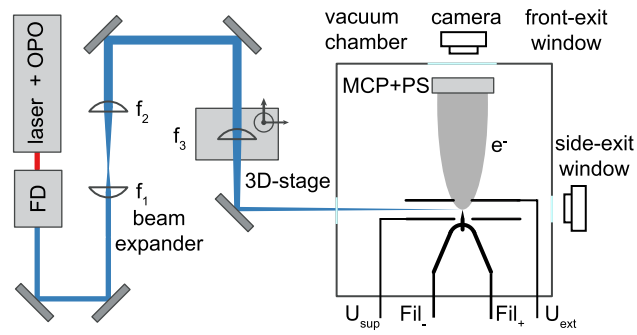


Fig. 2 Experimental setup. The laser beam from a femtosecond-oscillator pumped optical parametric oscillator is frequency doubled (FD), expanded (two convex lenses with $f_1 = 35$ mm and $f_2 = 125$ mm) and focused (achromatic lens with $f_3 = 400$ mm on a nanopositioning 3D-stage) onto a W(310)-nanotip. The tip is mounted in a Schottky-type emitter assembly consisting of a suppressor and an extractor anode. For flashing of the tip, a current can be applied between the two filaments Fil_+ and Fil_- ; for control over electron emission, the suppressor voltage U_{sup} is fixed at the tip potential and the extractor electrode is biased with U_{ext} . The electron emission is recorded on an imaging microchannel plate (MCP) with a subsequent phosphor screen (PS)

voltage U_{ext} at the tip apex $E_{\text{tip}} = \frac{U_{\text{ext}}}{kr}$ is locally enhanced by the geometric form factor of the emitter assembly k and the radius of curvature of the nanotip r . In this model, the tunneling current $j(E_{\text{tip}}, \phi)$ from a material with the work function ϕ is described by the Fowler–Nordheim equation [66]

$$j(E_{\text{tip}}, \phi) = \frac{e^3 E_{\text{tip}}^2}{8\pi h \phi t^2} \exp \left[-\frac{8\pi \sqrt{2m}\phi^{3/2}}{3heE_{\text{tip}}} v \right]. \quad (1)$$

Here, e is the elementary charge, m is the electron mass and the special field emission elliptic functions $v \approx 1-f(E_{\text{tip}}, \phi)+(1/6)f(E_{\text{tip}}, \phi)\ln f(E_{\text{tip}}, \phi)$ and $t \approx 1+(1/9)f(E_{\text{tip}}, \phi)-(1/18)f(E_{\text{tip}}, \phi)\ln f(E_{\text{tip}}, \phi)$ are slowly varying functions of $f(E_{\text{tip}}, \phi) = (e^3/4\pi\epsilon_0)(E_{\text{tip}}/\phi^2)$ [66–68]. The Fowler–Nordheim equation describes both FE and PFE processes with the work functions ϕ and ϕ_λ , respectively.

3 Experimental setup

The wavelength- and field-dependent emission current from a cold field emitter is experimentally studied with the setup shown in Fig. 2. A W(310)-nanotip is mounted in a Schottky-type emitter assembly [69, 70], consisting of a suppressor and an extractor, mounted inside a vacuum chamber at a base pressure of $5 \cdot 10^{-11}$ mbar. The tip is flash-cleaned by applying ~ 3 A current pulses of a few seconds to the filaments Fil_+ and Fil_- while no high-tension is applied to the electrodes. Next, the tip voltage U_{tip} (the voltage applied to the shorted filaments), the extractor voltage U_{ext} and the

suppressor voltage U_{sup} are ramped up simultaneously to a beam voltage of -4 kV relative to the vacuum chamber at ground potential. FE is induced by increasing U_{ext} . The electron emission pattern is amplified by a Chevron-type micro-channel plate (MCP) and recorded with a phosphor screen and camera. The electron current is retrieved by integrating the image intensity.

A high-contrast of PFE versus FE current is observed for optical illumination of the tip with low bias voltage U_{ext} . The frequency-doubled output of a femtosecond-pumped optical parametric oscillator (OPO) generates wavelength-tunable laser pulses with a pulse duration of 100 fs at a repetition rate of about 80 MHz. The laser beam is expanded with a telescope and focused with an achromatic lens onto the apex of the nanotip (230 nm radius of curvature, cf. Fig. 3c & SI), resulting in a focal spot size of $80 \times 20 \mu\text{m}^2$. The light polarization is aligned parallel to the tip, and the laser focus position is optimized with a 3D-nanopositioning-stage for maximum emission current. For the few-femtoampere currents observed in photoemission mode, an emission half-time of 30 min is found, generally governed by the vacuum level at the emitter. Environmental gases adsorbed on the

surface of the nanotip can be reversibly removed by flashing, fully recovering the current [71].

4 Photoassisted cold field emission

Localization of the photoelectron emission to the apex region is verified by raster scanning the laser focus over the emitter (cf. Fig. 3a–c). Figure 3a shows an *in-situ* transmission image of the tip in the emitter assembly with a camera placed behind the side-exit window of the vacuum chamber. A raster scan of the laser focus over the tip (shown in Fig. 3b) correlates the local electron yield with the transmitted laser power measured at the side-exit window. The laser-power transmission map matches the *in-situ* and SEM (cf. Fig. 3c) images of the emitter, the former being primarily blurred by the laser focal spot size. A comparison of Figs. 3a, b shows peak photoemission from the apex, with a weaker tail towards the shaft.

The laser-power scaling of the photoemission current is plotted in Fig. 3d. A linear fit to the data clearly verifies one-photon photoemission. The total emission current

$$j_{\text{full}}(E_{\text{tip}}, \phi, \lambda) = a_{\text{FE}} j(E_{\text{tip}}, \phi) + a_{\text{PFE}} j(E_{\text{tip}}, \phi, \lambda) \quad (2)$$

is a sum of contributions from FE (high tip electric fields, weight factor a_{FE}) and PFE (low tip electric fields, weight factor a_{PFE}).

Fowler–Nordheim-type plots and their fits to Eq. 2 are shown in Fig. 4a for data sets without illumination and with laser excitation at different wavelengths. The photoemission curves are normalized to the incident laser power. As expected, the curve without optical illumination has a constant slope over the measurement range, related to the emitter geometry and work function. In contrast, while having the same slope at high extraction fields (FE regime), the photoemission data sets exhibit a strongly increased current at lower extraction fields (PFE regime). This results in a decreased slope in the PFE regime and is directly linked to a decrease of the effective work function ϕ_{λ} that depends on the laser wavelength (cf. Eq. 1). In a transition regime at intermediate extraction voltages, the measured current is increasingly dominated by FE for rising extraction fields. For a reduced photon energy (smaller ϕ_{λ}), the slope of the PFE component is reduced, and the intersection between the fits of the FE and PFE components is shifted to lower U_{ext} . Tuning the laser wavelength λ from 500 nm to 400 nm while keeping the time-averaged laser power P_{avg} constant increases the photoemission contrast (the ratio of fitted PFE versus FE current) by approximately three orders of magnitude over the extraction voltages in the measurement range (see Fig. 4b).

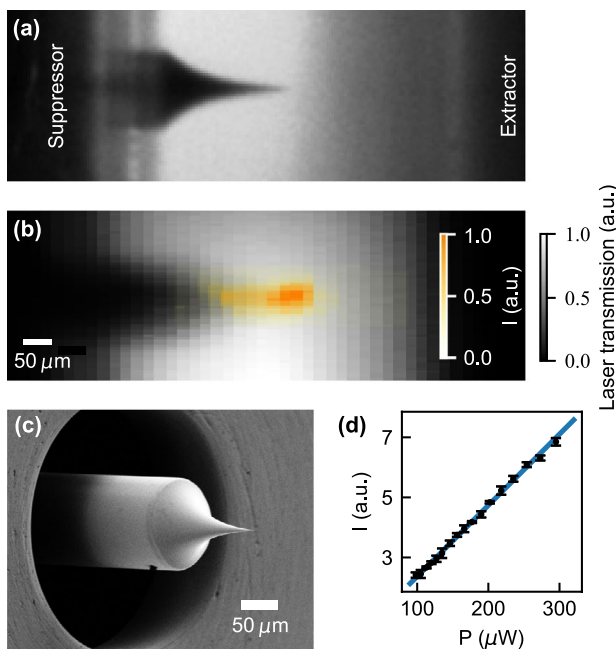


Fig. 3 Nanotip photoemission. **a** Transmission image of the emitter assembly. **b** Overlay of the laser-position-dependent electron current (colorscale) onto the local laser transmission (gray-scale). Parameters used in the experiment: $P_{\text{laser}} = 100 \mu\text{W}$, $\lambda_{\text{laser}} = 400 \text{ nm}$ and $U_{\text{ext}} - U_{\text{tip}} = 1750 \text{ V}$. **c** Scanning electron microscope picture of the W(310)-nanotip with the suppressor in the background recorded. **d** Linearly fitted photoemission current for varying laser power between $100 \mu\text{W}$ and $300 \mu\text{W}$ (same U_{ext} , λ as in **b**). The data points and error bars are calculated from the mean and root mean square current of three 300-ms images

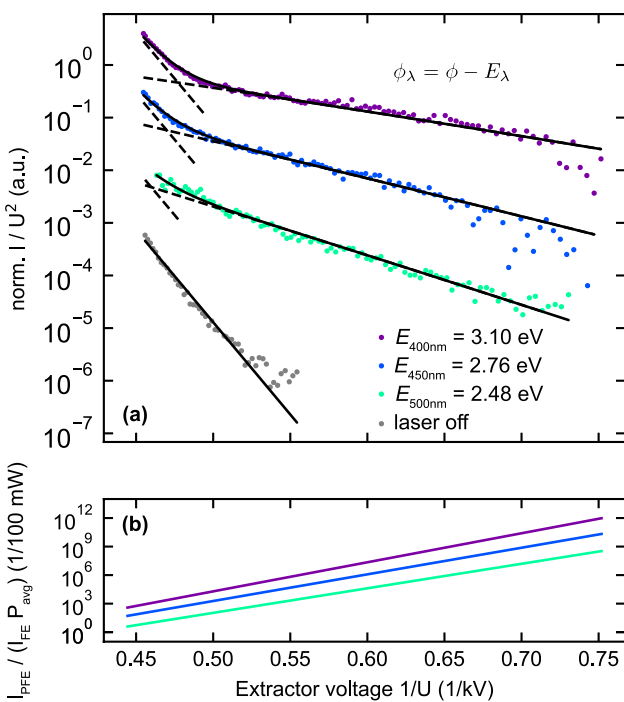


Fig. 4 Fowler–Nordheim plots and photoemission contrast. **a** Fitted logarithmic currents divided by the squared extraction voltage for field emission without illumination (laser off) and photoemission (laser wavelengths $\lambda = 500, 450, 400 \text{ nm}$ at time-averaged laser powers $P_{\text{avg}} = 20, 0.7, 0.14 \text{ mW}$, respectively) against the inverse extraction voltage. The photoemission data sets are normalized to the incident laser power on the nanotip, and the field emission data set is shifted relative to the photoemission data sets for visibility; the FE and PFE components of the joint fits are visualized separately using dashed lines. **b** Ratio of fitted PFE versus FE current at laser wavelengths from panel (a) normalized to an incident time-averaged laser power P_{avg} of 100 mW

To retrieve the global parameters ϕ and r , a joint model using four equations of type Eq. (2) is employed and fitted to the data shown in Fig. 4a. The FE and high-current part of the PFE data are assigned higher fit weights accounting for their lower noise. For each curve, the parameters a_{FE} and a_{PFE} are retrieved separately ($a_{\text{PFE}} = 0$ without optical illumination), with effective work functions ϕ_λ . The global fit yields a work function of $\phi = 4.32 \pm 0.04 \text{ eV}$ and an effective tip radius of curvature of $r = 224 \pm 6 \text{ nm}$ using a geometric form factor of the emitter assembly $k = 5.9$, which was estimated from finite element simulations of the emitter geometry (see SI).

The fitted work function ϕ is in excellent agreement with the literature value of $\phi_{\text{W(310)}} = 4.35 \text{ eV}$ [72]. The extracted radius of curvature r agrees with SEM images of the repeatedly flashed and thereby dulled emitter acquired after the experiments ($r = 230 \text{ nm}$, see SI). For all laser wavelengths, the experimentally measured currents are well-described by PFE theory with an effective work function reduced by the photon-energy.

5 Conclusion

In conclusion, we study photoassisted field emission from a W(310)-nanotip using low-power femtosecond excitation, controlling the effective work function by tuning the laser wavelength. Our results combine the flexibility of linear photoemission with femtosecond gating and the high beam coherence from cold field emitters. Improved vacuum conditions and active wavelength feedback may be used to extend the emission lifetime. Future work will involve a quantitative characterization of the electron beam brightness and kinetic energy distributions in UTEM. The linear photoemission process offers tailored temporal and spectral characteristics of the emitted electron pulses. These parameters may enable advanced electron phase-space control using, for example, chirped optical pulses in future high-coherence UTEM instruments.

Supplementary Information The online version of this article (<https://doi.org/10.1007/s00340-023-07968-2>) contains supplementary material, which is available to authorized users.

Acknowledgements This work was funded by the Deutsche Forschungsgemeinschaft (DFG, German Research Foundation) through 217133147/SFB 1073, project A05 and the Gottfried Wilhelm Leibniz program. We gratefully acknowledge support from the Göttingen UTEM team. Furthermore, we thank M. Reutzel and N. Hertl for useful discussions and B. Schröder and M. Sivis for assistance with the acquisition of SEM images.

Funding Open Access funding enabled and organized by Projekt DEAL.

Data availability statement The data that support the findings of this study are available from the corresponding author upon reasonable request.

Declarations

Conflict of interest The authors have no conflict of interest to disclose.

Open Access This article is licensed under a Creative Commons Attribution 4.0 International License, which permits use, sharing, adaptation, distribution and reproduction in any medium or format, as long as you give appropriate credit to the original author(s) and the source, provide a link to the Creative Commons licence, and indicate if changes were made. The images or other third party material in this article are included in the article's Creative Commons licence, unless indicated otherwise in a credit line to the material. If material is not included in the article's Creative Commons licence and your intended use is not permitted by statutory regulation or exceeds the permitted use, you will need to obtain permission directly from the copyright holder. To view a copy of this licence, visit <http://creativecommons.org/licenses/by/4.0/>.

References

1. K.B. Schliep, P. Quartermann, J.-P. Wang, D.J. Flannigan, *Appl. Phys. Lett.* **110**, 222404 (2017). <https://doi.org/10.1063/1.4984586>
2. N. Rubiano da Silva, M. Möller, A. Feist, H. Ulrichs, C. Ropers, S. Schäfer, *Phys. Rev. X* **8**, 031052 (2018). <https://doi.org/10.1103/physrevx.8.031052>
3. M. Möller, J.H. Gaida, S. Schäfer, C. Ropers, *Commun. Phys.* **3**, 36 (2020). <https://doi.org/10.1038/s42005-020-0301-y>
4. D.R. Cremons, D.A. Plemmons, D.J. Flannigan, *Struct. Dyn.* **4**, 044019 (2017). <https://doi.org/10.1063/1.4982817>
5. A. Feist, N. Rubiano da Silva, W. Liang, C. Ropers, S. Schäfer, *Struct. Dyn.* **5**, 014302 (2018). <https://doi.org/10.1063/1.5009822>
6. N. Bach, A. Feist, M. Möller, C. Ropers, S. Schäfer, *Struct. Dyn.* **9**, 034301 (2022). <https://doi.org/10.1063/4.0000144>
7. M.S. Grinolds, V.A. Lobastov, J. Weissenrieder, A.H. Zewail, *Proc. Natl. Acad. Sci. USA* **103**, 18427 (2006). <https://doi.org/10.1073/pnas.0609233103>
8. R.M. van der Veen, O.-H. Kwon, A. Tissot, A. Hauser, A.H. Zewail, *Nat. Chem.* **5**, 395 (2013). <https://doi.org/10.1038/nchem.1622>
9. T. Danz, T. Domröse, C. Ropers, *Science* **371**, 371 (2021). <https://doi.org/10.1126/science.abd2774>
10. B. Barwick, D.J. Flannigan, A.H. Zewail, *Nature* **462**, 902 (2009). <https://doi.org/10.1038/nature08662>
11. A. Feist, K.E. Echternkamp, J. Schauss, S.V. Yalunin, S. Schäfer, C. Ropers, *Nature* **521**, 200 (2015). <https://doi.org/10.1038/nature14463>
12. T.R. Harvey, J.-W. Henke, O. Kfir, H. Lourenço-Martins, A. Feist, F.J. García de Abajo, C. Ropers, *Nano Lett.* **20**, 4377 (2020). <https://doi.org/10.1021/acs.nanolett.0c01130>
13. I. Madan, G. M. Vanacore, E. Pomarico, G. Berruto, R. J. Lamb, D. McGrouther, T. T. A. Lummen, T. Latychevskaia, F. J. García de Abajo, F. Carbone, *Sci. Adv.* **5**, eaav8358 (2019). <https://doi.org/10.1126/sciadv.aav8358>
14. X. Fu, E. Wang, Y. Zhao, A. Liu, E. Montgomery, V. J. Gokhale, J. J. Gorman, C. Jing, J. W. Lau, Y. Zhu, *Sci. Adv.* **6**, eabc3456 (2020). <https://doi.org/10.1126/sciadv.abc3456>
15. Y. Kurman, R. Dahan, H.H. Sheinfux, K. Wang, M. Yannai, Y. Adiv, O. Reinhardt, L.H.G. Tizei, S.Y. Woo, J. Li, J.H. Edgar, M. Kociak, F.H.L. Koppens, I. Kaminer, *Science* **372**, 1181 (2021). <https://doi.org/10.1126/science.abg9015>
16. D.J. Flannigan, A.H. Zewail, *Acc. Chem. Res.* **45**, 1828 (2012). <https://doi.org/10.1021/ar3001684>
17. L. Piazza, D. Masiel, T. LaGrange, B. Reed, B. Barwick, F. Carbone, *Chem. Phys.* **423**, 79 (2013). <https://doi.org/10.1016/j.chemphys.2013.06.026>
18. A. Feist, N. Bach, N. Rubiano da Silva, T. Danz, M. Möller, K.E. Priebe, T. Domröse, J.G. Gatzmann, S. Rost, J. Schauss, S. Strauch, R. Bormann, M. Sivis, S. Schäfer, C. Ropers, *Ultramicroscopy* **176**, 63 (2017). <https://doi.org/10.1016/j.ultramic.2016.12.005>
19. H. Dömer, O. Bostanjoglo, *Rev. Sci. Instrum.* **74**, 4369 (2003). <https://doi.org/10.1063/1.1611612>
20. W.E. King, G.H. Campbell, A. Frank, B. Reed, J.F. Schmerge, B.J. Siwick, B.C. Stuart, P.M. Weber, *J. Appl. Phys.* **97**, 111101 (2005). <https://doi.org/10.1063/1.1927699>
21. J.S. Kim, T. LaGrange, B.W. Reed, M.L. Taheri, M.R. Armstrong, W.E. King, N.D. Browning, G.H. Campbell, *Science* **321**, 1472 (2008). <https://doi.org/10.1126/science.1161517>
22. P. Hommelhoff, Y. Sortais, A. Aghajani-Talesh, M.A. Kasevich, *Phys. Rev. Lett.* **96**, 077401 (2006). <https://doi.org/10.1103/PhysRevLett.96.077401>
23. C. Ropers, D.R. Solli, C.P. Schulz, C. Lienau, T. Elsaesser, *Phys. Rev. Lett.* **98**, 043907 (2007). <https://doi.org/10.1103/PhysRevLett.98.043907>
24. B. Barwick, C. Corder, J. Strohaber, N. Chandler-Smith, C. Uiterwaal, H. Batelaan, *New J. Phys.* **9**, 142 (2007). <https://doi.org/10.1088/1367-2630/9/5/142>
25. H. Yanagisawa, M. Hengsberger, D. Leuenberger, M. Klöckner, C. Hafner, T. Greber, J. Osterwalder, *Phys. Rev. Lett.* **107**, 087601 (2011). <https://doi.org/10.1103/PhysRevLett.107.087601>
26. D. Ebner, J. Hammer, M. Eisele, M. Krüger, J. Noe, A. Högele, P. Hommelhoff, *Phys. Rev. Lett.* **114**, 227601 (2015). <https://doi.org/10.1103/PhysRevLett.114.227601>
27. A. Tafel, S. Meier, J. Ristein, P. Hommelhoff, *Phys. Rev. Lett.* **123**, 146802 (2019). <https://doi.org/10.1103/PhysRevLett.123.146802>
28. L. Arnoldi, M. Borz, I. Blum, V. Kleshch, A. Obraztsov, A. Vella, *J. Appl. Phys.* **126**, 045710 (2019). <https://doi.org/10.1063/1.5092459>
29. D.-S. Yang, O.F. Mohammed, A.H. Zewail, *Proc. Natl. Acad. Sci. USA* **107**, 14993 (2010). <https://doi.org/10.1073/pnas.1009321107>
30. F. Houdellier, G. Caruso, S. Weber, M. Kociak, A. Arbouet, *Ultramicroscopy* **186**, 128 (2018). <https://doi.org/10.1016/j.ultramic.2017.12.015>
31. C. Zhu, D. Zheng, H. Wang, M. Zhang, Z. Li, S. Sun, P. Xu, H. Tian, Z. Li, H. Yang, J. Li, *Ultramicroscopy* **209**, 112887 (2020). <https://doi.org/10.1016/j.ultramic.2019.112887>
32. P.K. Olshin, M. Drabbels, U.J. Lorenz, *Struct. Dyn.* **7**, 054304 (2020). <https://doi.org/10.1063/4.0000034>
33. B. Cook, M. Brongseest, K. Hagen, P. Kruit, *Ultramicroscopy* **109**, 403 (2009). <https://doi.org/10.1016/j.ultramic.2008.11.024>
34. L. Swanson and G. Schwind, *Adv. Imaging Electron Phys.* **159**, 63 (2009). [https://doi.org/10.1016/S1076-5670\(09\)59002-7](https://doi.org/10.1016/S1076-5670(09)59002-7)
35. F. Houdellier, A. Masseboeuf, M. Monthoux, M.J. Hjorth, *Carbon* **50**, 2037 (2012). <https://doi.org/10.1016/j.carbon.2012.01.023>
36. H. Zhang, J. Tang, J. Yuan, Y. Yamauchi, T.T. Suzuki, N. Shinya, K. Nakajima, L.-C. Qin, *Nat. Nanotechnol.* **11**, 273 (2016). <https://doi.org/10.1038/nnano.2015.276>
37. C.W. Johnson, A.K. Schmid, M. Mankos, R. Röpke, N. Kerker, E.K. Wong, D.F. Ogletree, A.M. Minor, A. Stibor, *Phys. Rev. Lett.* **129**, 244802 (2022). <https://doi.org/10.1103/PhysRevLett.129.244802>
38. G. Pozzi, *Optik* **77**, 69 (1987)
39. M. J. G. Lee, *Phys. Rev. Lett.* **30**, 1193 (1973). <https://doi.org/10.1103/PhysRevLett.30.1193>
40. M. Zani, V. Sala, G. Irde, S.M. Pietralunga, C. Manzoni, G. Cerullo, G. Lanzani, A. Tagliaferri, *Ultramicroscopy* **187**, 93 (2018). <https://doi.org/10.1016/j.ultramic.2018.01.010>
41. B. Schröder, O. Bunjes, L. Wimmer, K. Kaiser, G.A. Traeger, T. Kotzott, C. Ropers, M. Wenderoth, *New J. Phys.* **22**, 033047 (2020). <https://doi.org/10.1088/1367-2630/ab74ac>
42. P. Dombi, Z. Pápa, J. Vogelsang, S. V. Yalunin, M. Sivis, G. Herink, S. Schäfer, P. Groß, C. Ropers, C. Lienau, *Rev. Mod. Phys.* **92**, 025003 (2020). <https://doi.org/10.1103/RevModPhys.92.025003>
43. J.L. Reynolds, Y. Israel, A.J. Bowman, B. B. Klopfer, M. A. Kasevich *Phys. Rev. Applied* **19**, 014035 (2023). <https://doi.org/10.1103/PhysRevApplied.19.014035>
44. D. Venus, M. Lee, *Surf. Sci.* **116**, 359 (1982). [https://doi.org/10.1016/0039-6028\(82\)90439-3](https://doi.org/10.1016/0039-6028(82)90439-3)
45. S. Liu, M. Wolf, T. Kumagai, *Phys. Rev. Lett.* **121**, 226802 (2018). <https://doi.org/10.1103/PhysRevLett.121.226802>
46. M.H. Mammez, M. Borz, I. Blum, S. Moldovan, L. Arnoldi, S. Idlahcen, A. Hideur, V.I. Kleshch, A.N. Obraztsov, A. Vella, *New J. Phys.* **21**, 113060 (2019). <https://doi.org/10.1088/1367-2630/ab5857>

47. M. Schenk, M. Krüger, P. Hommelhoff, Phys. Rev. Lett. **105**, 257601 (2010). <https://doi.org/10.1103/physrevlett.105.257601>
48. M. Krüger, M. Schenk, P. Hommelhoff, Nature **475**, 78 (2011). <https://doi.org/10.1038/nature10196>
49. P. Hommelhoff, C. Kealhofer, M.A. Kasevich, Phys. Rev. Lett. **97**, 247402 (2006). <https://doi.org/10.1103/PhysRevLett.97.247402>
50. R. Bormann, M. Gulde, A. Weismann, S.V. Yalunin, C. Ropers, Phys. Rev. Lett. **105**, 147601 (2010). <https://doi.org/10.1103/PhysRevLett.105.147601>
51. G. Herink, D.R. Solli, M. Gulde, C. Ropers, Nature **483**, 190 (2012). <https://doi.org/10.1038/nature10878>
52. L. Wimmer, G. Herink, D.R. Solli, S.V. Yalunin, K.E. Echternkamp, C. Ropers, Nat. Phys. **10**, 432 (2014). <https://doi.org/10.1038/nphys2974>
53. G. Herink, L. Wimmer, C. Ropers, New J. Phys. **16**, 123005 (2014). <https://doi.org/10.1088/1367-2630/16/12/123005>
54. J. Houard, L. Arnoldi, A. Ayoub, A. Hideur, A. Vella, Appl. Phys. Lett. **117**, 151105 (2020). <https://doi.org/10.1063/5.0022182>
55. K.E. Echternkamp, G. Herink, S.V. Yalunin, K. Rademann, S. Schäfer, C. Ropers, Appl. Phys. B **122**, 80 (2016). <https://doi.org/10.1007/s00340-016-6351-x>
56. H. Boersch, Z. Physik **139**, 115 (1954). <https://doi.org/10.1007/BF01375256>
57. B. Cook, T. Verduin, C.W. Hagen, P. Kruit, J. Vac. Sci. Technol. B **28**, c6c74 (2010). <https://doi.org/10.1116/1.3502642>
58. M. Kuwahara, Y. Nambo, K. Aoki, K. Sameshima, X. Jin, T. Ujihara, H. Asano, K. Saitoh, Y. Takeda, N. Tanaka, Appl. Phys. Lett. **109**, 013108 (2016). <https://doi.org/10.1063/1.4955457>
59. B. Cook and P. Kruit, Appl. Phys. Lett. **109**, 151901 (2016). <https://doi.org/10.1063/1.4963783>
60. N. Bach, T. Domröse, A. Feist, T. Rittmann, S. Strauch, C. Ropers, S. Schäfer, Struct. Dyn. **6**, 014301 (2019). <https://doi.org/10.1063/1.5066093>
61. H. Yanagisawa, T. Greber, C. Hafner, J. Osterwalder, Phys. Rev. B **101**, 045406 (2020). <https://doi.org/10.1103/PhysRevB.101.045406>
62. J. Schotz, L. Seiffert, A. Maliakkal, J. Blochl, D. Zimin, P. Rosenberger, B. Bergues, P. Hommelhoff, F. Krausz, T. Fennel, M. F. Kling, Nanophotonics **10**, 3769 (2021). <https://doi.org/10.1515/nanoph-2021-0276>
63. S. Meier and P. Hommelhoff, ACS Photonics **9**, 3083 (2022). <https://doi.org/10.1021/acsphtronics.2c00839>
64. R. Haindl, A. Feist, T. Domröse, M. Möller, S. V. Yalunin, C. Ropers, [arXiv:2209.12300](https://arxiv.org/abs/2209.12300) (2022).
65. R. H. Fowler and L. Nordheim, Proc. R. Soc. Lond. A **119**, 173 (1928). <https://doi.org/10.1098/rspa.1928.0091>
66. R. G. Forbes and J. H. Deane, Proc. R. Soc. A. **463**, 2907 (2007). <https://doi.org/10.1098/rspa.2007.0030>
67. J.H.B. Deane and R.G. Forbes, J. Phys. A: Math. Theor. **41**, 395301 (2008). <https://doi.org/10.1088/1751-8113/41/39/395301>
68. S.V. Filippov, E.O. Popov, A.G. Kolosko, J. Vac. Sci. Technol. B **39**, 044002 (2021). <https://doi.org/10.1116/6.0000960>
69. R. Bormann, S. Strauch, S. Schäfer, C. Ropers, J. Appl. Phys. **118**, 173105 (2015). <https://doi.org/10.1063/1.4934681>
70. B. Schröder, M. Sivis, R. Bormann, S. Schäfer, C. Ropers, Appl. Phys. Lett. **107**, 231105 (2015). <https://doi.org/10.1063/1.493721>
71. K. Kasuya, S. Katagiri, T. Ohshima, S. Kokubo, J. Vac. Sci. Technol. B **28**, L55 (2010). <https://doi.org/10.1116/1.3488988>
72. H. Kawano, Prog. Surf. Sci. **83**, 1 (2008). <https://doi.org/10.1016/j.progsurf.2007.11.001>

Publisher's Note Springer Nature remains neutral with regard to jurisdictional claims in published maps and institutional affiliations.